Two-Dimensional Melting Transition Observed in a Block Copolymer

D. E. Angelescu,* C. K. Harrison,† M. L. Trawick, R. A. Register, and P. M. Chaikin
Departments of Physics, Chemical Engineering, PRISM-Princeton University, Princeton, New Jersey 08544, USA
(Received 27 June 2004; published 8 July 2005)

We report the observation of two-dimensional melting in a monolayer film of a sphere-forming diblock copolymer. By annealing in a well-controlled temperature gradient we obtain a complete record of the transition from a low-temperature hexatic phase to a high-temperature liquid in a single experiment. We investigate the temperature dependence of the orientational and translational correlation lengths, as well as of the topological defect density. All evidence suggests that the melting transition is first-order, but correlations in the liquid phase indicate the existence of an underlying second-order transition preempted by the first-order freezing.

DOI: 10.1103/PhysRevLett.95.025702 PACS numbers: 64.70.Dv, 68.37.Ps

Two-dimensional melting has been an area of intense research and continuous debate over the past three decades. Several theoretical models, computer simulations, and experimental studies have been dedicated to the subject of melting in two dimensions, with predictions and results that are often contradictory [1]. The most popular theory of two-dimensional melting is the Kosterlitz-Thouless-Halperin-Nelson-Young theory (KTHNY) [2–4], which describes a two-step melting scenario for two-dimensional crystals: a first step, caused by the unbinding of dislocations, leads from the 2D crystalline to a hexatic phase, while the second, higher-temperature, step leads from the hexatic to the isotropic liquid phase and is caused by the unbinding of disclinations. The three phases can be described in terms of their correlation functions: the 2D crystalline phase has long-range orientational and *quasi-long-range* translational correlations, the hexatic phase has *quasi-long-range* orientational and short-range translational correlations whereas the isotropic liquid phase has short-range correlations for both. Both the transitions are predicted to be second-order in the KTHNY model, but competing theories exist which propose different melting scenarios [5–7]. In computer simulations the transition is seen to depend critically on model parameters [8–10]; liquid-solid coexistence is reported in some simulations [11]. Recent experimental work on two-dimensional melting focuses on model systems [12–19], where precise positional data can be acquired via microscopy. In the present Letter we describe the two-dimensional melting transition in a monolayer film of a diblock copolymer forming spherical microdomains, and suggest that it is first order in nature.

Our sample consisted of a thin film of polystyrene-*b*-poly(ethylene-alt-propylene) (PS-PEP) synthesized by living anionic polymerization followed by hydrogenation. The molecular weights of the blocks were 3.3 kg/mol (PS) and 23.1 kg/mol (PEP) [20], leading to an equilibrium morphology consisting of spherical PS microdomains spaced 25 nm apart within a matrix of PEP, with bcc symmetry in bulk and hexagonal symmetry in thin-film samples. The bulk order-disorder transition temperature T_{ODT} was measured as $121 \pm 2\,^{\circ}C$ and the upper glass transition temperature (PS block) was $\approx 40\,^{\circ}C$. PS-PEP films 30 nm thick, corresponding to a monolayer of microdomains, were obtained by spin coating from dilute (ca. 1%) polymer solutions onto oxide-coated Si strips. Such films exhibit a brushlike wetting layer ($\approx$10 nm thick) underlying the microdomains, with the PS blocks adsorbed at the Si interface, as demonstrated by dynamical secondary-ion mass spectrometry [21]. The morphology of the film is shown schematically in Fig. 1(b) (inset).

The film-coated substrate was suspended between two heaters with temperatures fixed above and below T_{ODT}, producing a temperature gradient which resulted in a linear mapping between the annealing temperature and the position along the sample (a similar approach, involving a density gradient, was successfully used in the study of two-dimensional melting in colloidal model systems in the pioneering work of Murray and Van Winkle [12]). On-sample temperatures were continuously recorded during the anneal by resistive temperature sensors microfabricated onto the sample substrate, and were stable within $0.2\,^{\circ}C$. To avoid polymer degradation, the anneals were performed in N_2 under constant overpressure. Subsequent to the anneal, the samples were rapidly quenched by immersion in liquid N_2. In order to ''freeze'' the microdomain configuration, samples were stored, subsequent to the anneal, in a freezer at $-27\,^{\circ}C$, until the AFM investigation could be performed.

Micrographs of the microdomain lattice were acquired by tapping-mode atomic force microscopy (TM-AFM, Digital Instruments Dimension 3000). $2.5 \times 2.5\ \mu m^2$ phase imaging micrographs of the triangular microdomain lattice were acquired every 250 μm (along the temperature gradient direction) in the melting transition region, which corresponded to a micrograph every $0.4\,^{\circ}C$. The colder end of the sample displayed an ordered lattice [Fig. 1(a) shows a characteristic portion of such a scan], whereas the hot end displayed a completely melted lattice [Fig. 1(b)]; the transition was located approximately in the middle of the sample. Standard computational algorithms [21] were employed to locate topological defects and calculate orienta-

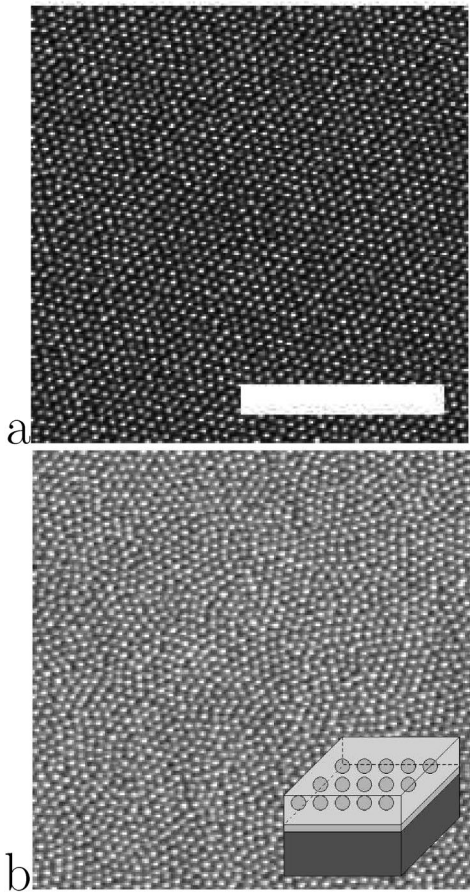

FIG. 1. Thin-film samples of PS-PEP 3–24, annealed below [panel (a), $T = 116.4\,^{\circ}\mathrm{C}$] and above [panel (b), $T = 144.1\,^{\circ}\mathrm{C}$] T_{ODT}. The white dots are spherical PS microdomains. The microdomain lattice shown in panel (a) is crystalline; in panel (b) it is melted to the isotropic liquid state. Scale bar: 250 nm. The inset in panel (b) is a schematic of the thin-film morphology of the copolymer, showing a monolayer of microdomains with a wetting layer at the Si interface.

tional correlation functions $g_6(r)$. Higher magnification $1.25 \times 1.25\ \mu\mathrm{m}^2$ micrographs were analyzed similarly, using the increased precision in locating the microdomain centers to calculate positional correlation functions $g_G(r)$. Large scale ($10 \times 10\ \mu\mathrm{m}^2$) micrographs were used to obtain large scale lattice orientational data, by employing an aliasing technique [22] previously developed.

The orientation of the lines connecting the centers of neighboring spheres defined the bond-orientational order parameter field $\Theta(\mathbf{r}_b)$ where $\mathbf{r}_b$ is the center of each bond. The orientational correlation functions were computed using

$$g_6(r) = \langle \cos\{6[\Theta(\mathbf{r}_0) - \Theta(\mathbf{r}_0 + \mathbf{r})]\}\rangle_{\mathbf{r}_0,\hat{\mathbf{r}}} \qquad (1)$$

where the averaging was done over all directions ($\hat{\mathbf{r}}$) and all locations ($\mathbf{r}_0$). Orientational correlation functions decayed exponentially above the melting transition, so that orientational correlation lengths ξ_6 could be calculated from $g_6(r) = \exp(-r/\xi_6)$.

The dependence of the bond-orientational correlation length ξ_6 on temperature is shown in Fig. 2(a). On the high-temperature side of the graph, correlation lengths are very small, revealing a complete lack of orientational order. This corresponds to annealing far above the melting transition, where the microdomain lattice is completely disordered. This disordered state is an equilibrium one: continued annealing does not enhance the ordering in this region, as verified in the inset to Fig. 2(a), where data from 4-hour and 35-hour anneals superimpose perfectly over 127–145 °C.

The low-temperature ($T < 112\,^{\circ}\mathrm{C}$) side of the graph in Fig. 2(a) shows a similar lack of order, but of a nonequilibrium origin: the decrease in molecular mobility with

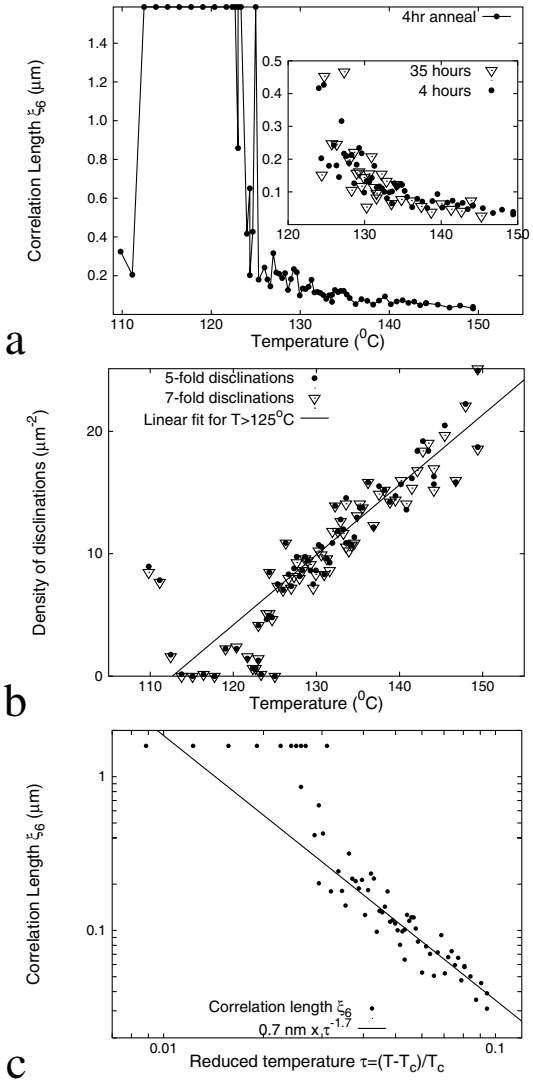

FIG. 2. Panel (a) Orientational correlation lengths after a 4-hour anneal. Inset displays overlapping data from the 4-hour and 35-hour anneals. Panel (b) Density of fivefold and sevenfold disclinations. Linear fit for $T > 125.5\,^{\circ}\mathrm{C}$ also shown. Panel (c) Log-log plot of the correlation length vs reduced temperature τ, consistent with power-law behavior (best fit shown).

decreasing temperature, especially as the glass transition of the PS block is approached. When annealed longer, these regions of the sample show an increasing degree of orientational order.

The middle region of the graph displays the melting transition, and represents the main focus of this Letter. Here, we notice a slow increase in orientational correlation length ξ_6 as temperature decreases from 150 °C. This gradual increase in ξ_6 ceases at $T = 125.5$ °C, where a sudden jump in correlation length occurs. Over the next 2.5 °C (in the 123–125.5 °C temperature range), we notice significant fluctuations of the correlation length suggesting alternating well-ordered and melted regions. As temperature is further decreased, the size of the well-ordered regions becomes comparable to, or larger than the size of the 2.5×2.5 μm^2 AFM scans, which implies nondecaying correlation functions, or ''infinite'' orientational correlation lengths. The points on the upper line of the graph in Fig. 2(a) correspond to such single-grain regions.

We have also examined the dependence on annealing temperature of the density of disclinations, which are topological defects responsible for orientational disorder. Figure 2(b) shows the graph of disclination density vs temperature, which also exhibits a discontinuity near 125 °C, indicative of first-order melting. Above the transition, however, both the correlation length and the disclination density exhibit the continuous behavior characteristic of a second-order transition. The disclination density displays a linear increase above the melting transition temperature (125 °C); if extrapolated to lower temperatures, the intercept with the temperature axis would correspond to a critical temperature $T_c = 113.0$ °C (386.1 K), 12 °C below the discontinuity. Investigating the dependence of the correlation length on reduced temperature $\tau = (T - T_c)/T_c$ above the melting transition reveals roughly power-law behavior, visible on the log-log plot in Fig. 2(c).

The scatter of the data for $\tau > 0.032$ ($T > 125.5$ °C) in Fig. 2(c) is indicative of the errors in calculating correlation lengths from AFM micrographs: all the data points lie in a $\pm 50\%$ band. This error arises from the limited number of grains in each micrograph. For the data points on the upper line of the graph (at $\tau < 0.026$, $T < 123$ °C), the AFM micrographs consistently displayed single grains larger than the size of the image; consequently, no error estimate is available, but the quoted value of $\xi_6 = 1.5$ μm is a conservative lower bound. Thus, in the intermediate temperature region ($0.026 < \tau < 0.032$, $123\,°\text{C} < T < 125.5\,°\text{C}$), the observed fluctuations in ξ_6 are much larger than any errors associated with its measurement.

In order to study translational correlation functions, 1.25×1.25 μm^2 micrographs were acquired in very large single crystal regions, so that the revealed structure approached the equilibrium configuration. In order to analyze these micrographs, the images were first Fourier transformed, and the six first-order peaks in the Fourier transform corresponding to the triangular lattice were located with high accuracy, using a centroid construction. The particle displacement field was defined as $\mathbf{u}(\mathbf{r}) = \Sigma_m \mathbf{r}\delta(\mathbf{r} - \mathbf{r}_m)$ (with $\mathbf{r}_m$ being the positions of the microdomain centers), and positional correlation functions were computed:

$$g_G(r) = \frac{1}{6}\sum_{i=1,6}\langle\cos\{\mathbf{G}_i \cdot [\mathbf{u}(\mathbf{r}_0) - \mathbf{u}(\mathbf{r}_0 + \mathbf{r})]\}\rangle_{\mathbf{r}_0,\hat{\mathbf{r}}} \quad (2)$$

where the averaging is again done over $\hat{\mathbf{r}}$ (the direction of $\mathbf{r}$), over all locations within the image, $\mathbf{r}_0$ and over $\mathbf{G}_i$. We have examined the translational correlation functions in the region just below the melting transition ($110\,°\text{C} < T < 123\,°\text{C}$) for distances up to 15 lattice spacings; AFM thermal drift distortions [23] rendered translational correlation calculations unreliable for larger distances. The correlation functions (Fig. 3) decayed exponentially for all anneal temperatures investigated, suggesting that *quasi-long-range* translational order was not present. The melting transition leads therefore from the hexatic to the liquid phase. The exponential decay was fast ($\xi_G \approx 4$ lattice spacings) close to the orientational melting transition, slower ($\xi_G \approx 8$ lattice spacings) in the intermediate range and fast again ($\xi_G \approx 3$ lattice spacings) closer to 110 °C, where molecular mobility is reduced.

As mentioned above, from 123 to 125.5 °C the correlation functions revealed alternating well-ordered and poorly ordered regions. The most striking illustration of these fluctuations comes from 10×10 μm^2 micrographs. Figure 4 shows portions of two such micrographs, taken 60 μm from each other (and corresponding to annealing temperatures of 124.7 and 124.8 °C, respectively). The colder region shows a single grain with size larger than 5 μm $\times$ 5 μm, whereas the hotter region shows numerous 1 μm $\times$ 1 μm grains. These large fluctuations in grain size around the melting transition, reflected in Fig. 2(a),

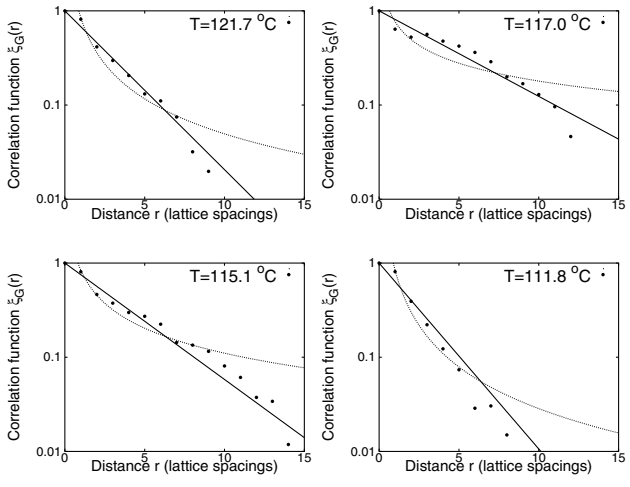

FIG. 3. Translational correlation functions $\xi_G(r)$ (4-hour anneal). Exponential (solid line) and power-law (dotted line) least square fits to the data are shown; the exponential functional form provides a better fit over the whole temperature range (110–123 °C).

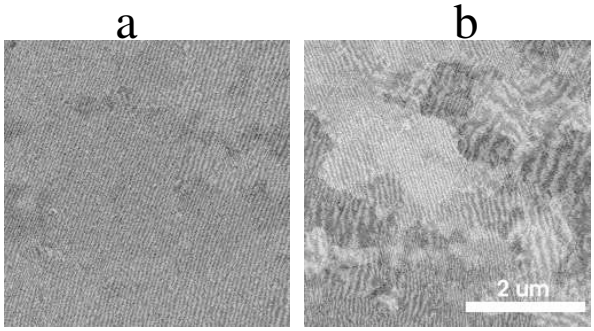

FIG. 4. Fluctuations between well-ordered and poorly ordered regions visible in portions of $10 \times 10\ \mu m^2$ micrographs. Picture (a) shows a single grain larger than 5 μm. Picture (b), taken 60 μm away, shows numerous grains of $\approx 1\ \mu$m diameter. The line patterns result from aliasing in the AFM image, with different patterns corresponding to different grain orientations presented in different shades of gray (details elsewhere [21,22]).

could be observed directly in the micrographs even after much longer anneals. It is important to note that such fluctuations may not be noticed unless a significant number of images is acquired close to the melting transition.

Such fluctuations could arise from local variations in the melting temperature, of order 1 °C over the 100 μm length scale, which could result from minute variations in film thickness over this length scale. Another possibility is that the small grains' growth is kinetically limited, due to the existence of nanometer-scale defect pinning sites on the substrate. Either of these effects could produce the observed coexistence, for a first-order transition; in any case, this observation cannot be accounted for if the transition is smoothly second order.

The evidence presented suggests that the two-dimensional melting transition occurs at $T = 125\,^{\circ}C$ (very close to the bulk T_{ODT}) and leads from a phase with hexatic order to a liquidlike phase, *via* a first-order transition. A second, lower temperature transition from 2D crystal to hexatic was not observed; we believe it was masked by the reduction in molecular mobility below 110 °C, where the crystal is hindered from forming. Our finding of a first-order transition is consistent with published experimental work [15], computer simulations results [10], and theoretical predictions [24] for selected systems.

It does, however, differ from the finding of Segalman and co-workers [19], for polystyrene-*b*-(2-vinylpyridine) thin films. Those authors found a continuous melting (hexatic-liquid) transition as described by the KTHNY theory, with a transition temperature significantly lower than the bulk T_{ODT}. An important distinction is that the substrates employed by Segalman *et al.* were micropatterned to topographically confine the microdomains, which significantly influences the transition [25] by producing preferential orientation even in the liquid state. In addition, the temperature gradient approach described in this Letter permits the acquisition of an arbitrarily large density of images close to the transition; while the behavior at high temperatures reflects an underlying second-order transition (Fig. 2), consistent with the KTHNY scenario, sampling the system close to the melting point reveals its true first-order nature.

We gratefully acknowledge support from the National Science Foundation through the Princeton Center for Complex Materials (DMR-0213706).

*Present address: Schlumberger-Doll Research, 36 Old Quarry Rd., Ridgefield, CT 06877, USA
†Present address: Schlumberger-Doll Research, 36 Old Quarry Rd., Ridgefield, CT 06877, USA

[1] K. J. Strandburg, Rev. Mod. Phys. **60**, 161 (1988).
[2] J. M. Kosterlitz and D. J. Thouless, J. Phys. C **6**, 1181 (1973).
[3] D. R. Nelson and B. I. Halperin, Phys. Rev. B **19**, 2457 (1979).
[4] A. P. Young, Phys. Rev. B **19**, 1855 (1979).
[5] S. T. Chui, Phys. Rev. B **28**, 178 (1983).
[6] H. Kleinert, Phys. Lett. A **95**, 381 (1983).
[7] V. N. Ryzhov and E. E. Tareyeva, Physica A (Amsterdam) **314**, 396 (2002).
[8] Y. Saito, Phys. Rev. B **26**, 6239 (1982).
[9] K. J. Strandburg, Phys. Rev. B **34**, 3536 (1986).
[10] P. Bladon and D. Frenkel, Phys. Rev. Lett. **74**, 2519 (1995).
[11] S. Toxvaerd, Phys. Rev. Lett. **44**, 1002 (1980).
[12] C. A. Murray and D. H. Van Winkle, Phys. Rev. Lett. **58**, 1200 (1987).
[13] Y. Tang, A. J. Armstrong, R. C. Mockler, and W. J. O'Sullivan, Phys. Rev. Lett. **62**, 2401 (1989).
[14] R. E. Kusner, J. A. Mann, J. Kerins, and A. J. Dahm, Phys. Rev. Lett. **73**, 3113 (1994).
[15] A. H. Marcus and S. A. Rice, Phys. Rev. Lett. **77**, 2577 (1996).
[16] K. Zahn, R. Lenke, and G. Maret, Phys. Rev. Lett. **82**, 2721 (1999).
[17] P. Karnchanaphanurach, B. H. Lin, and S. A. Rice, Phys. Rev. E **61**, 4036 (2000).
[18] R. Seshadri and R. M. Westervelt, Phys. Rev. B **46**, 5142 (1992).
[19] R. A. Segalman, A. Hexemer, R. C. Hayward, and E. J. Kramer, Macromolecules **36**, 3272 (2003).
[20] J. M. Sebastian, C. Lai, W. W. Graessley, and R. A. Register, Macromolecules **35**, 2707 (2002).
[21] D. E. Angelescu, Ph.D. thesis, Princeton University, 2003.
[22] D. E. Angelescu, C. K. Harrison, M. L. Trawick, P. M. Chaikin, R. A. Register, and D. H. Adamson, Appl. Phys. A **78**, 387 (2004).
[23] M. L. Trawick, M. Megens, C. Harrison, D. E. Angelescu, D. A. Vega, P. M. Chaikin, R. A. Register, and D. H. Adamson, Scanning **25**, 25 (2003).
[24] T. Chou and D. R. Nelson, Phys. Rev. E **53**, 2560 (1996).
[25] R. A. Segalman, A. Hexemer, and E. J. Kramer, Phys. Rev. Lett. **91**, 196101 (2003).